Title
Validating predictive models for fast ion profile relaxation in burning plasmas

Journal
Nuclear Fusion, 56(11)

ISSN
0029-5515

Authors
Gorelenkov, NN
Heidbrink, WW
Kramer, GJ
et al.

Publication Date
2016-11-01

DOI
10.1088/0029-5515/56/11/112015

IOP Publishing | International Atomic Energy Agency Nuclear Fusion

Nucl. Fusion **56** (2016) 112015 (10pp) doi:10.1088/0029-5515/56/11/112015

Validating predictive models for fast ion profile relaxation in burning plasmas

N.N. Gorelenkov[1], W.W. Heidbrink[2], G.J. Kramer[1], J.B. Lestz[1], M. Podesta[1], M.A. Van Zeeland[3] and R.B. White[1]

[1] Princeton Plasma Physics Laboratory, Princeton, NJ, USA
[2] University of California, Irvine, CA, USA
[3] General Atomics, San Diego, CA, USA

E-mail: ngorelen@pppl.gov

Received 12 January 2016, revised 10 June 2016
Accepted for publication 23 June 2016
Published 22 July 2016

Abstract

The redistribution and potential loss of energetic particles due to MHD modes can limit the performance of fusion plasmas by reducing the plasma heating rate. In this work, we present validation studies of the 1.5D critical gradient model (CGM) for Alfvén eigenmode (AE) induced EP transport in NSTX and DIII-D neutral beam heated plasmas. In previous comparisons with a single DIII-D L-mode case, the CGM model was found to be responsible for 75% of measured AE induced neutron deficit [1]. A fully kinetic HINST is used to compute mode stability for the non-perturbative version of CGM (or nCGM). We have found that AEs show strong local instability drive up to $\gamma/\omega \sim 20\%$ violating assumptions of perturbative approaches used in NOVA-K code. We demonstrate that both models agree with each other and both underestimate the neutron deficit measured in DIII-D shot by approximately a factor of 2.

On the other hand in NSTX the application of CGM shows good agreement for the measured flux deficit predictions. We attempt to understand these results with the help of the so-called kick model which is based on the guiding center code ORBIT. The kick model comparison gives important insight into the underlying velocity space dependence of the AE induced EP transport as well as it allows the estimate of the neutron deficit in the presence of the low frequency Alfvénic modes. Within the limitations of used models we infer that there are missing modes in the analysis which could improve the agreement with the experiments.

Keywords: alpha particles, Alfvénic modes, magnetic fusion, reduced quasi-linear model

(Some figures may appear in colour only in the online journal)

1. Introduction

The fast ion (or energetic particle—EP) confinement is one of the key problems to be addressed in preparation for future burning plasma (BP) experiments [2, 3] such as ITER [4]. EPs are expected in fusion plasmas to compensate the energy loss due to various transport processes and thus needed for self-sustained burning plasma operations.

Fast ions can efficiently resonate with the Alfvénic modes in finite beta plasmas, which is a major concern for planned burning plasma (BP) experiments as discussed in several recent review papers [2, 3, 5]. The EP confinement problem can be understood by developing reduced EP transport models which capture the main physics of wave-particle interactions (WPI) [3]. The problem of EP profiles relaxation due to Alfvénic modes is investigated here using primarily the critical gradient model (CGM) developed recently [6]. CGM approach is the limiting case of the quasi-linear (QL) models [7] when the number of modes goes to infinity and the fast ion diffusion is fast. In other words CGM is the marginal stability limit of QL model.

The CGM modifies higher moments of EP distribution function, such as their pressure or density assuming that the

distribution function is slowing down above and below the fundamental Alfvénic resonance velocity. The model is relatively simple as it is based on the perturbative linear stability theory of AEs. The stability theory was a subject of recent validating exercises by the ITPA group [8] where EP drive as a function of the ratio of the fast ion orbit width to the mode width was computed by several different codes. Earlier CGM (also called here the 1.5D model) applications [6, 9] reasonably well described such integral parameters as EP pressure profiles. This encouraged further validation against recent DIII-D experiments at elevated $q_{\min}$ values [1]. The application of CGM included the comparison of time averaged EP predicted pressure profiles over the interval comparable with the fast ion slowing down time. Despite such averaging, the agreement obtained between the experiments and predictions was surprisingly good. However the employed averaging masks details of the EP distribution profiles and their dynamics to make more definite conclusion about the possible CGM applications or suggestion for its improvement.

In this paper we attempt a systematic validation of CGM against a broader range of plasma parameters such as DIII-D and NSTX discharges which are prone to AE instabilities. We choose the time intervals between the analyzed points which are shorter than the slowing down time as will be discussed in section 4 but sufficiently long to change the instability rates. The CGM application resulted in its under-prediction of the neutron losses in DIII-D by approximately a factor of two whereas CGM provided a reasonable agreement for the NSTX shot within the expeimental error bars. Integrated plasma modeling of analyzed discharges of two devices is provided by the plasma analysing code TRANSP [10].

In order to understand the discrepancy we apply the so-called 'kick' model [11] to the same data. We confirm the CGM under-prediction for analyzed DIII-D shot if only Alfvénic modes are assumed to cause EP transport. The kick model suggests that adding the instabilities with the frequencies lower than TAE's, which are indeed observed in the experimental frequency spectrum, can eliminate the neutron deficit discrepancy.

Our paper is organized as follows. In section 2 we describe the approaches we are using for EP relaxation in the presence of the Alfvénic modes. Section 3 is devoted to the NSTX experiments and the next section 4 describes DIII-D plasma conditions chosen for the analyses. The comparison against the kick model simulation is given in section 5. The summary of the results is given in section 6.

2. Approaches used

2.1. Critical gradient models

The 1.5D model was described in detail recently [6] and is based on the earlier idea to compute the critical (radial) gradient of EP density due to AE instabilities in order to estimate the relaxed EP profiles [12]. We should mention that the CGM concept could be found even in earlier publications such as [13, 14]. See more discussion about the CGM relationship to possible nonlinear scenarios in [2], where CGM profiles are referred to as 'marginal distribution' in figure 27 of that reference. That paper points out at the CGM as a plausible scenario in the presence of a system of unstable modes (not necessarily Alfvénic).

CGM predicts the EP pressure profiles by finding the background plasma damping of stable and unstable AEs and thus is weakly dependent on the AE instability nonlinear dynamics. Even though CGM could not resolve all the details of EP fast ion distribution function the model itself is consistent with the measured EP profiles in DIII-D where they were almost independent on the injection geometry [1]. We note that CGM can be considered as a limiting case (the marginal stability limit) of the QL approach for strong collisional plasmas, i.e. when the background plasma damping rates are balanced by the growth rates due to the EP component. Strong collisions mean that the extent of the resonance island is large in radial direction and that the resonances can easily overlap even with very low mode amplitudes. Thus the requirement of a large number of modes can be generalized to large number of overlapped resonances in the presence of a few AEs. This regimes, often met in experiments, correspond to near threshold excitation of AE instabilities when the collisional scattering is much larger than the resonant particle 'bounce' frequency, i.e. the bounce of trapping frequency in the AE mode fields. It is hard to quantify the conditions when the CGM is expected to work in experiments for the reasons of experimental uncertainties in the number of instabilities and in their internal amplitudes which could be a sensitivity issue for the diagnostics.

As the framework of the CGM prescribes [6, 12] we perform a linear stability analysis of the TAEs/RSAEs (toroidicity induced AEs or reversed shear AEs). A key expression of 1.5D CGM balances the beta gradient of the fast ions when the AEs are near the excitation threshold locally, i.e. $\gamma_d = \gamma_f$ where linear growth and damping rates equal each other. Then we can write

$$\left(a\frac{\partial\beta_f}{\partial r}\right)_{\rm crit} = \frac{\gamma_d}{\gamma_f^*}. \qquad (1)$$

Here β_f is the fast ion beta at a mode location, γ_f is the linear growth rate in the absence of dissipation and γ_d is the damping rate without the destabilizing source. Here the linear growth rate is assumed to be of the form $\gamma_f = \gamma_f^* a(\partial_r\beta_f)$ with γ_f^* taken as independent of the energetic particle beta profile. Hence in the region encompassing the unstable modes we require that the AE instability relaxation will result in $\left|\partial\beta_f/\partial r\right| \leqslant \left|\partial\beta_f/\partial r\right|_{\rm crit}$. In other words, if the EP gradient predicted by transport codes such as TRANSP [10] is larger than the critical value, the EP profile is relaxed to the critical value by the 1.5D CGM model. This enables an integration of the gradient, equation (1), and a subsequent computation of the fast ion beta profile. Comparing the CGM relaxed and initial beta profiles results in the computation of EP profile redistribution outside the initially unstable region to those regions

where the AEs are stable initially. In addition, if the broadened profiles reach the plasma edge CGM can predict losses.

In this paper we present two different methods to compute the relaxed EP profiles via critical gradients. The first one is the perturbative CGM or pCGM. In this case the ideal MHD code, NOVA, computes TAE or RSAE mode structures [6]. The second method is the non-perturbative CGM (or nCGM) and is based on calculations using the HIgh-n STability kinetic ballooning code—HINST [15, 16]. The comparison of several models in this paper is based on the calculations of the neutron rates. In CGM models it is computed as an integral of the product of beam and thermal plasma densities using the assumtion that the fusion cross section does not change as a function of beam ion energy [6]. We illustrate the accuracy of used approximation for the neutron deficit in section 5 making use of the kick model which is integrated into the TRANSP code.

The last assumption seems to be sufficient for the validation exercise of this paper. Neverthless it is known that this approximation can be corrected for realistic computations of energetic injected beams with finite thermal ion temperature of the background plasma [17] as well as it can be corrected for the effect of AE redistribution in the velocity space, not just in radius, [18]. Let us demonstrate that both approximations do not change the neutron deficit we are computing.

The first effect [17] leads to the cross section increase by the factor $\delta S \sim (1 + 3T_i/E_f)$, where T_i is thermal ion temperature and E_f is beam injection energy. In DIII-D and NSTX these corrections are small, 11% and 4%, respectively. The second effect is shown to lead to changes in the fusion reaction rate caused by the fast ion energy change associated with the energy transport induced by TAEs [18]. In this paper we use the following definition of the neutron deficit in the perturbative and nonperturbative CGMs as

$$S_{\text{deficit}} = (S_{\text{classical}} - S_{\text{computed}})/S_{\text{classical}}, \qquad (2)$$

where $S_j \sim n_{fj} n_i \sigma_{DD}(E_f) v_f$, n_{fj} and S_j are the corresponding densities of fast ions and sources of neutrons with j being the 'classical' or 'computed'. This expression of the neutron deficit masks the inaccuracy in the assumption for the fusion cross-section as long as both functions, $S_{\text{classical}}$ and S_{computed}, are evaluated using the same weighting for the fast ions, i.e. the same distribution function for the initial and relaxed fast ion distributions. Witnin the versions of CGM used here we find that the resonances are broad in the phase space (see an example of such resonances in [19]). To resolve them one would need the velocity space resolution beyond the simple dominant Alfvénic resonance considered in [6].

Other contribution to the neutron signal deficit may include the charge exchange loss associated with the presence of neutral gas mostly at the plasma edge. However careful estimate of this effect done within TRANSP shows its contribution to equation (2) is negligible for both devices.

2.1.1. Perturbative CGM using NOVA-K code. 1.5D pCGM has the option to improve its accuracy by employing the normalization of the growth and damping rates using the NOVA-K code [20] rather then analytic, less accurate expressions. For pCGM the integrated plasma simulation transport code TRANSP [10] is typically used. With these modifications 1.5D model accurately captures TAE or RSAE (also called Alfvén Cascades [21]) structures and their stability properties.

We normalize the growth/damping rates so that the applied analytic rate expressions are multiplied by the ratio $\gamma_{\text{NOVA}}(r_i)/\gamma_{\text{anlt}}(r_i)$ at a radial point r_i. Then linear interpolated or extrapolated rates are used between the normalization points whereas outside of those points the analytic rates are computed. Dominant dampings are thermal electron and ion Landau, and trapped electron collisional dampings which were the focus of recent validation exercises [8, 22]. At observed low to medium values of the toroidal mode numbers ($n = 3$–6 on both devices) other damping mechanisms are less important, such as radiative and continuum dampings. More accurate continuum damping rate calculations are available in the non-perturbative version of NOVA [23].

The growth rates of the Alfvénic modes include finite orbit width and Larmor radius effects. This allows implementation a special procedure for the normalization [6], which finds the most unstable AE over different toroidal mode numbers. In DIII-D and NSTX experiments, the number of normalization radial points varies from 4 to 5 for $n \sim 3$–6.

Let us demonstrate normalization of a special procedure using two point normalization. One finds the most unstable modes over possible n values, localized near two radial points, r_1 and r_2, $r_1 < r_2 < a$, where a is the plasma minor radius. Analytically computed rates are multiplied by a constant g_1 for $r < r_1$ so that it coincides with the value given by NOVA-K at r_1, and the procedure is identical for $r > r_2$ with the multiplier g_2. For $r_1 < r < r_2$ the rate is multiplied by a linear function $ar + b$ so that $ar_1 + b = g_1$ and $ar_2 + b = g_2$. Thus the multiplier g_i is a ratio of NOVA-K computed increments/decrements sum to the analytic values.

When the NOVA-K code computes the increment due to fast ions it allows the variation of the ion charge, $0 < z_\alpha < \sim 20$. This is equivalent to changing the ratio of AE radial width to EP orbit width Δ_m/Δ_f, where $\Delta_f = q\rho_f$ and $\Delta_m \approx r_m/m$, q is the safety factor, ρ_f is the fast ion Larmor radius, r_m is the minor radius of TAE location, and m is the characteristic poloidal mode number. As the theory predicts [24, 25] and computations confirm [20], the dependence of the AE growth rate on z_α has the plateau near the maximum growth value. It is then used to estimate the required AE growth rate. A special study was done to understand if this procedure is sensitive to the choice of n or mode location. It was found that the presence of the plateau helps to justify this procedure [12].

The assumed slowing down EP distribution function in CGM/1.5D model does not resolve the velocity space dynamics appropriately. CGM assumes that only passing particles are contributing to the relaxation. In cases of DIII-D and NSTX plasmas all the beam ions are injected superalfvenic and are included in the redistribution. The EP distribution function assumes the single source of the beam ions at one injection pitch angle and velocity. This is sufficient for realistic collisional broadening in pitch angles as was shown earlier [12].

2.1.2. Non-perturbative CGM using HINST calculations. As we will see the pCGM has two properties which are hard to reconcile with experiments. First is that the growth rates due to beam ions of TAE/RSAE modes are often large, $\gamma_f/\omega \sim 10\%$, which is beyond the perturbative approach. The second property in DIII-D is that there are indications of measured TAE radial structures to be in agreement with non-perturbative calculations. The measurements of the characteristic width of the mode is shown to be about two times narrower in simulations than in linear perturbative analysis and has similar width to the mode width obtained by the ideal MHD code [26]. This motivated us to develop the non-perturbative version of CGM (or nCGM) where TAEs are computed by the non-perturbative code HINST (HIgh-n STability) [15, 16].

Thus the non-perturbative AEs are expected to rely on the non-perturbative simulations by the HINST code which can find the eigenfrequency and the growth rates. Many shortcomings of NOVA-K analysis are properly resolved by the HINST code such as the radiative damping and EP growth rates in the non-perturbative regime. We note that the code was recently used to study the stability of AEs in ITER and demonstrated to be consistent with NOVA-K computations [12].

HINST code solves the set of AE equations using the shooting technique in the ballooning variable which is the poloidal angle extended to infinity [27]. The formulation of this code is presented in [16]. HINST finds the required perturbed variables: electrostatic potential Φ, parallel electric field potential Ψ and perturbed parallel magnetic field, $\delta B_\parallel$. If plasma oscillations have strong acoustic branch present such as in the case of low frequency kinetic ballooning modes (KBMs) all three quantities have to be included when finding the solutions [16].

2.2. Kick model approach

The recently developed kick model [11] is used here for detailed modeling of AE induced redistribution in order to help verify and validate CGM predictions. The model connects the detailed interpretation of the measured EP transport with their dynamics in the phase space. It includes the ORBIT guiding center code EP drift orbit computations [28], i.e. realistic particle trajectories in the presence of several plasma oscillations of TAE/RSAE modes. The TAE/RSAE radial and poloidal structures are inferred from the experimental measurements.

The kick model is designed to improve the deficiency of standard TRANSP plasma simulations for tokamaks where the EP transport in the phase space has limited flexibility. In nominal TRANSP runs it is considered uniform and independent of the ion pitch angle and energy. There the velocity space diffusion is described by the ad-hoc radial diffusion coefficient $D_b(t)$ used by the NUBEAM package [29] implemented in TRANSP. Kick model prescribes the diffusion coefficient which is a function of particle phase space position as follows.

The formalism of this model is based on the Hamiltonian Lorentz force equation for the variation of beam ion energy and toroidal angular momentum

$$\omega P_\varphi - n\mathcal{E} = \text{const.}, \tag{3}$$

i.e. $\Delta P_\varphi/\Delta\mathcal{E} = n/\omega$, setting a constraint for EP motion in the phase space involving ion energy and toroidal angular momentum. The model main ingredient is the probability function $p(\Delta\mathcal{E}, \Delta P_\varphi|\mathcal{E}, P_\varphi, \mu)$ that the ion is characterized by the constants of motion (COM), $\mathcal{E}, P_\varphi, \mu$ in the phase space, to change its position by the mode. The kick model approach generalizes equation (3) in the presence of multiple resonances between fast ions and a mode at a given amplitude A. This approach allows to evolve the EP ensemble without resolving all fine details of fast ions in the phase space at the location of the EP resonances with the modes. An example of kick model applications is given in [30].

3. pCGM validation against NSTX experiments

We start validating the perturbative version of CGM against the NSTX shot #141711 presented in detail in [31]. The application of nCGM can be hardly justified in this device due to expected and observed low toroidal mode numbers of TAE frequency range instabilities whereas HINST formalism requires $n \gg 1$ as discussed in section 2.1.2.

The plasma parameters in this shot were: toroidal field $B_0 \simeq 0.5$T, typical density $n_e = (3-4)\times 10^{19}\,\mathrm{m}^{-3}$, and the plasma species temperatures $T_e \simeq T_i \lesssim 1.5$ keV with the plasma rotation of the order of 40 kHz. This machine has the main neutral beam (NB) heating system which typically results in the fast ion super-Alfvénic population at $1 < v_{h0}/v_A < 5$. EP typically drive the TAE modes and the variety of other modes. In the chosen plasma the safety factor is reversed in radius and evolves in time. Its minimum value decreases from 4 to unity and is reconstructed through the LRDFIT [32] code with the constraint of motional Stark effect (MSE) diagnostics measurements of the magnetic field inside the plasma. Overall uncertainties of the reconstruction are inferred from the measurement to be $\Delta q \simeq 0.1$.

The AE resonances in NSTX are broad in velocity space due to large orbit width effects and low toroidal mode numbers. Because of this the EP contributions are important not only from particles with dominant Alfvénic resonance $v_\parallel = v_A$ but at other harmonics $v_\parallel = v_A/(1+2l)$, $l > 0$. In NSTX plasma $v_{h0}/v_A = 2.3$ at $t = 470$ ms in the plasma center. EP are tangentially injected centered at the pitch angle $\chi_0 \equiv v_\parallel/v = 0.94$ with the width $\Delta\chi^2 = 0.1$.

We also apply the kick model which is based on the measured magnetic activity in the case of NSTX using an array of 11 Mirnov pick-up coils spread toroidally. Mirnov coil data is analyzed to compute the time-dependent frequency spectra. Figure 1 shows the evolution of different low to medium n frequency signals with the characteristic frequency chirping down on a msec time scale. The toroidal mode numbers are color coded in the figure as indicated. These instabilities are not virulent despite the chirping behavior. The choice of this shot is made due to its relatively benign AEs which transform to an avalanche at $t = 480$ ms as pointed out in [31]. We should note that the CGM is not applicable beyond $t = 480$ ms as the physics of EP transport in the avalanche is far more complicated than the model treats.

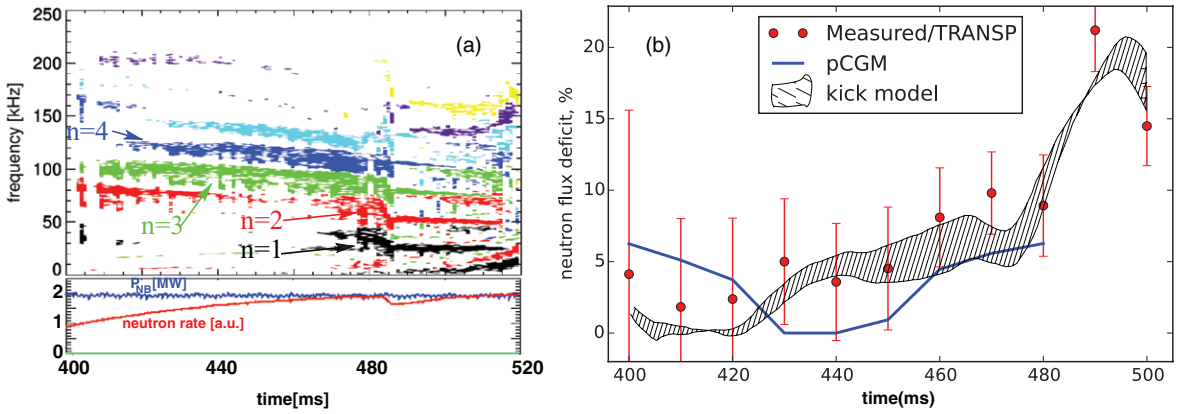

Figure 1. Figure (*a*) represents Mirnov coil measured and analyzed magnetic field oscillations spectrum vs time in NSTX discharge #141711. Toroidal mode numbers in the range $n = 1$–4 are indicated on figure (*a*). Bottom insert of that figure depicts NBI power (blue curve) and neutron flux (red curve) evolutions. Figure (*b*) corresponds to the results of pCGM model predictions (blue solid curve) for the neutron deficit in that shot. Figure (*b*) also shows the comparison with the deficit coming from TRANSP modeling with $D_b(t)$ (shown as red dots with vertical error bars). In addition on that figure we plot the neutron deficit described by the kick modeling as indicated. Error bars represent the uncertainty in the computed deficit, including different assumptions on equilibrium reconstruction.

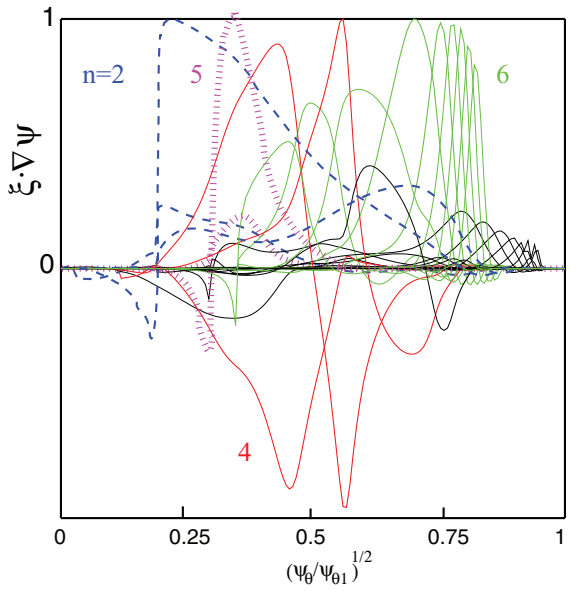

Figure 2. Poloidal harmonics of the representative TAE modes for $t = 470$ ms used in pCGM normalization for NSTX. The modes have the toroidal mode numbers color coded and shown on the plot. Plotted is the normal component of the plasma displacement normalized to one at its maximum point.

Table 1. Growth rates of TAEs used in pCGM simulations of NSTX at $t = 470$ ms.

r/a	0.17	0.232	0.336	0.41	0.53
γ_f/ω	0.138	0.01	0.0274	0.0073	0.0173
$-\gamma_d/\omega$	0.0043	0.0013	0.004	0.0002	0.0009
n	2	5	4	5	6
f, kHz	103	115.8	155.5	157.4	116.5

Note: The mode structures are shown in figure 2 except $n = 5$ TAE, $f = 157.4$ kHz, which is not in that figure. The table contains rows of the mode maximum locations r/a, growth rates γ_f/ω due to fast ions, sum of all the dominant damping rates, trapped electron collisional, thermal ion Landau and continuum/radiative damping rates, $-\gamma_d/\omega$, toroidal mode numbers, n, and the mode frequencies in kHz

The diffusion of fast ions in the TRANSP code is independent of particle pitch angle and velocity. However it is still helpful to compute the characteristic fast ion diffusion by matching the measurable quantities such as neutron flux with simulations. This approach results in the EP diffusion ranging within 0.1–1 $m^2\ s^{-1}$ given the experimental error bars for the neutron fluxes within ±5%. TRANSP diffusion during the avalanche, $t = 480$ ms, is inferred from experiments up to 8 $m^2\ s^{-1}$ to match the experimentally measured neutron flux.

Several times of interest were chosen for the analysis, $t = 400$–470 ms, separated by 10 ms. For each time comprehensive stability calculations were performed using NOVA-K code. Below, in figure 2 we show details of the analysis for one time, $t = 470$ ms, where radial structures of used TAEs are plotted. One can note that the mode structures are fairly broad and therefor are not prone to the discrete character of the mode stability calculations, i.e. when narrow unstable TAEs change their location and thus stability properties in radius when the safety factor slightly changes. This motivates the systematic study of CGM for a DIII-D case, as will be discussed in the next section.

We define the neutron flux deficit due to some mechanism as the flux in the presence of that mechanism divided by the 'classical' flux predicted by TRANSP in the absence of instabilities. The deficits resulting from measured neutron flux, pCGM predictions and kick model applications are shown in figure 1(*b*). Both pCGM and kick model simulations (discussed later in section 5) are within the experimental error bars.

NOVA-K performed stability analysis is summarized in the following table 1. The growth rate includes finite orbit width and Larmor radius effects via the formalism published in [20]. The same code is used to compute the thermal ion Landau damping. The plasma rotation is added to NOVA simulations using the approximation of a simple local Doppler shift in the eigenmode equations [33]. This allowed the computation of thermal ion Landau damping, which is strongly modified from its zero drift width expressions [34]. EP growth rate is also affected by the plasma rotation.

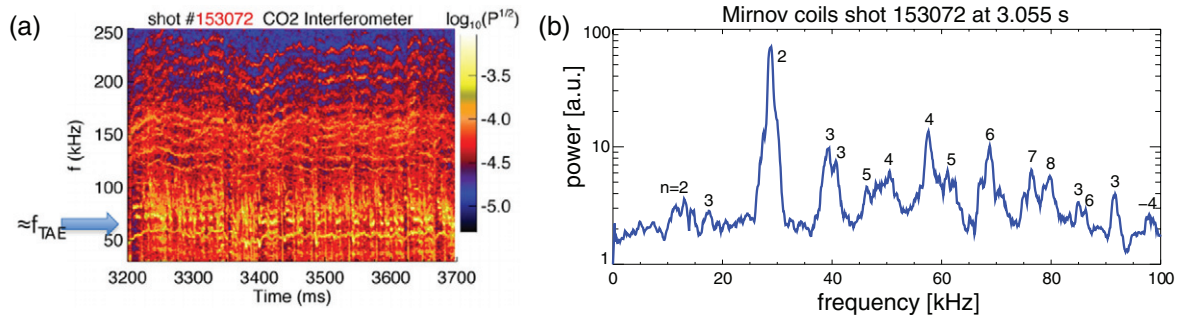

Figure 3. The time evolution of the magnetic signal spectra of DIII-D shot #153072, is shown in (*a*). Figure (*b*) depicts one time slice for these spectra where the toroidal mode numbers of each identified peak are also shown.

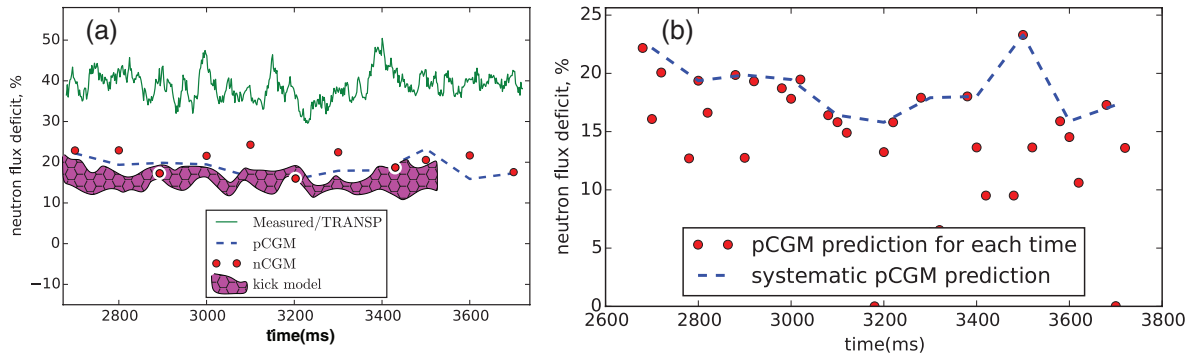

Figure 4. (*a*) The neutron deficit evolution over time, together with the pCGM computed deficit (dashed curve) and the kick model computations (lines with symbols). Critical gradient model predictions for neutron deficit in DIII-D #153072 shot are plotted on figure (*b*) as it emerges from the systematic study. The same curve is shown on both figures for comparisons. Shown as red dots are the pCGM computed points at all the times of the analyses.

pCGM relaxes EP beta profiles and the corresponding losses are computed by fixing the boundary condition for EP beta profile to zero at the plasma edge.

4. Perturbative and non-perturbative CGM validations against DIII-D experiments

4.1. Experiment

A DIII-D plasma of interest was extensively studied recently [35]. In cross section, it is a strongly shaped double-null diverter deuterium plasma heated by D beams. The plasma current, density, beam power were timed for the transition to the H-mode. A mixture of injecting beams at the tangential radii $R_{\rm tan} = 1.15$ m and $R_{\rm tan} = 0.76$ m was used at the nominal beam energy $E_f \simeq 80$ keV. The shot was steady-state and the safety factor profile was maintained reversed with the safety factor minimum at $r/a \simeq 0.2$. It was noted that in the analyzed campaign $q_{\rm min}$ played an important role by increasing the growth rates of the TAE modes. The injected pitch angle distribution is centered at $\chi_0 \equiv v_\parallel/v \simeq 0.5$, and the magnetic field on axis was $B_{\rm T} = 1.74$ T.

Strong Alfvénic activity was observed in this discharge as shown in the magnetic spectra, figure 3(*a*). It covers wide frequency range to well above the characteristic TAE frequency, up to 250 kHz. A snapshot of the spectrum taken at $t = 3.055$ s shows an example of descrete distinguished signals used in the analysis.

The neutron rate is below classical predictions in #153072 according to TRANSP simulations in the absence of AE driven transport. Using the same definition as above for the neutron deficit we plot it for the experimental signal on figure 4(*a*), which indicates almost steady neutron deficit over time at ∼40% level.

We should note that EP diffusion coefficient computed by CGM can not be summed in TRANSP with other diffusions algebraically since they account for the same physics. Because of this and because NOVA-K computations are perturbative we initiate simulations using TRANSP modeling which includes the ad-hoc diffusion coefficient $D_{\rm b}(t)$ as described in subsection 2.2 (we use the same TRANSP profiles for both perturbative and non-perturbative versions of CGM). The value of this coefficient is adjusted to the neutron flux to be close to measurements, ~ 2 m^2 s^{-1} over the time window of interest. As a result TAE growth rates computed by NOVA-K are relatively small as shown in the next section. The computed damping rates depend on the background plasma parameters only. Thus the EP critical gradient is within the perturbative assumptions.

4.2. pCGM application to DIII-D

We apply pCGM for DIII-D #153072 shot in a similar manner as we did for NSTX where we used 4 or 5 points in radius for normalization depending on the mode width and the stability results. However, here the model is used in a more systematic

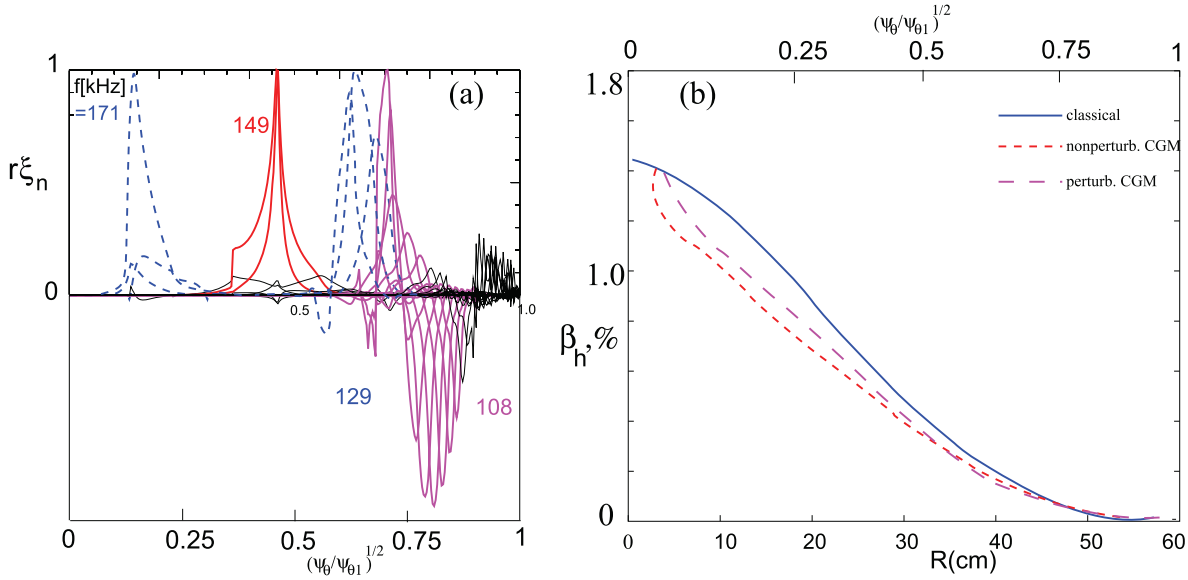

Figure 5. Figure (*a*) is for DIII-D #153072 discharge. It shows the same as figure 2 (drawn for NSTX #141711) but with all the modes plotted at $n = 5$, $t = 3.5$ s and their frequencies indicated near each mode structure. Figure (*b*) depicts the comparison between the beam ion profiles relaxation by pCGM and nCGM and how they are compared with the classical profile computed initially.

Table 2. Notations are the same as in table 1 but all for $n = 5$ from figure 5(*a*).

r/a	0.14	0.46	0.63	0.75
γ_f/ω	0.019	0.0114	0.049	0.038
$-\gamma_d/\omega$	0.002	0.0012	0.0047	0.001
f, kHz	171	149	129	108

way because of generally higher n's and narrower modes. At each chosen time t_0 (2.7, 2.8 and so on till 3.7 s) two nearby times were analyzed in addition, $t_0 \pm 10$ ms. Out of three times for each t_0 set the most unstable case is chosen to compute EP profiles and neutron deficit. This strategy reflects the discreteness of AE modes at certain safety factor profile. Thus one would expect that the AE transport is sensitive to the set of used eigenmodes and change drastically as q evolves.

We are showing an example of NOVA-K linear stability analysis in figure 5 for $t = 3.5$ s. The values of the growth and damping rates are summarized in table 2. One can note from the table that the modes are fairly unstable and yet the relaxed EP beta profiles are not modified strongly by the model near the plasma center. This is due to the extrapolation of thermal ion Landau damping to the center and its exponential dependence on the fast ion beta.

The time evolution of the neutron deficit from pCGM is shown in figures 4(*a*) and (*b*) as dashed curve. Figure 4(*b*) depicts possible variation of neutron deficit predictions at nearby times in the considered case. It also shows the amount of scattering due to the discreteness of the mode spectrum. As one can see from figure 4(*a*) pCGM predicts smaller deficit by the factor of two than the measured one. One possibility to reconcile the observations with the predictions of the pCGM is following. The mismatch results from our perturbative computations, namely TAE/RSAE structures are computed in NOVA-K without EP contributions. In their turn EPs are known to significantly modify the mode structure and its dispersion in DIII-D experiments [26]. The non-perturbative nature of the analysis results in more narrow and thus more unstable modes. Qualitatively this is because radially localized fast ion drive is sufficient for the localization of narrow Alfvénic low damped modes. We explore this idea in the next section.

4.3. nCGM application to DIII-D

For nCGM we utilize the HINST code to find the TAE net growth rate non-perturbatively. HINST is applied to DIII-D plasma where the drive can reach $\gamma_f/\omega \sim 0.3$ locally as shown in figure 6(*a*). HINST computed growth and damping rates are used for nCGM normalization. In nCGM the growth rates are interpolated between the HINST computed values. Beam ion neutron flux deficit is computed by the 1.5D CGM code plotted on figure 6(*b*).

The predictions of both pCGM and nCGM are close to each other even though the obtained growth rates by HINST are higher than NOVA-K rates. This is due to global mode structures of AEs in NOVA-K which average the local growth rate contributions over the mode structure.

5. Comparison with the kick model calculations

The kick model outlined in section 2.2 is applied here to the same plasma conditions as above. In NSTX TAE modes shown in figure 7(*a*) are used to construct the probability function. Kick model uses AE structures from NOVA calculations by comparing them with the reflectometer diagnostic so that the best fitted TAEs are implemented. Only few shown modes were used in the kick modeling. The measured displacements were measured at $t = 484$ ms where the signal is strongest and the error bars are minimal [31]. Plotted error bars represent the uncertainties in the inferred neutron rate deficit based

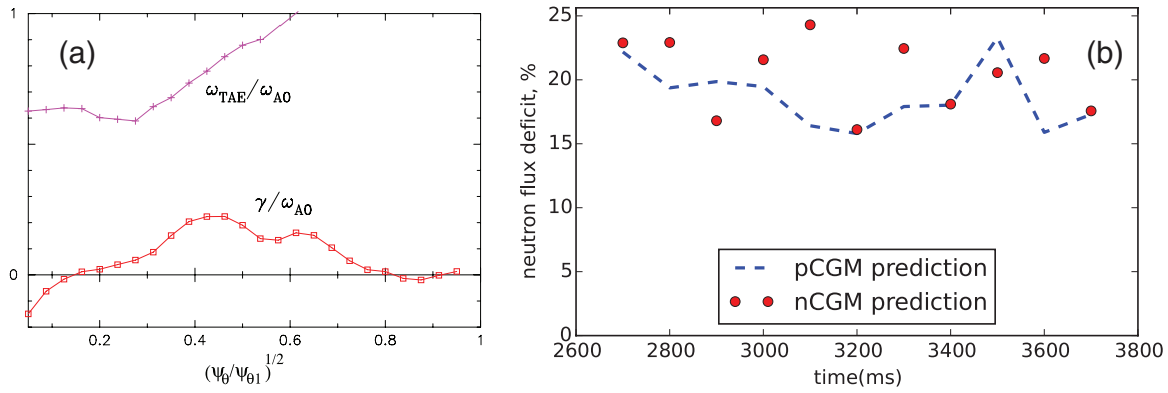

Figure 6. (*a*) Shows AE eigenfrequency (upper curve) denoted as ω_{TAE}/ω_{A0} and net growth rate, γ/ω_{A0}, from HINST calculations for DIII-D shot #153072, $t = 3.5$ s. A comparison of pCGM and nCGM predictions for neutron flux deficit.

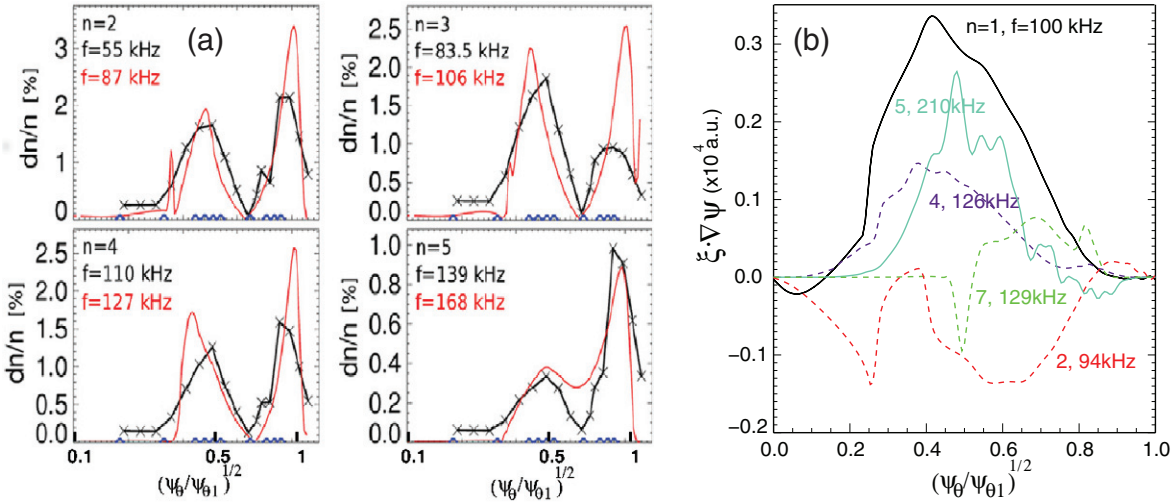

Figure 7. Figures (*a*) show plasma density perturbations, $\delta n/n$, used in the kick model for NSTX shot #141711 as computed by NOVA code (solid red lines). (*a*) also shows the comparison with the reflectometer measured plasma displacement (black solid lines with the *x* marks). (*b*) the plasma displacements found by NOVA code for largest amplitude modes in DIII-D plasma #153072. Each mode is marked by the toroidal mode number *n* and mode frequency in kHz.

on estimated ±5% uncertainty in the reflectometer measurements. Standard deviation of values from 10 ms time window used for binning experimental and TRANSP data is also added in quadrature.

In the kick model application to DIII-D the underlying AE measurements were taken at $t = 3.5$ s to construct 10 probability functions for NUBEAM. After that the diffusion coefficients were scaled according to measured magnetic fields at the edge. Figure 7(*b*) shows 5 used largest amplitude TAEs. The resulting neutron flux deficit from the kick model calculations is shown in figure 4(*a*) and is consistent with both pCGM and nCGM deficits. The applied models compute similar neutron deficit which is two times smaller than the measured neutron flux deficit. Analysis based on different equilibrium reconstructions through EFIT [36] or LRDFIT codes show similar results.

The kick modeling can not account for the low frequency activity seen in figure 3(*a*) below f_{TAE}, since NOVA could not find the appropriate solution in that frequency range. We conjecture here that those are the low frequency modes of Alfvénic acoustic nature or BAE or BAAE recently studied in [37]. They could explain the neutron flux deficit discrepancy. In fact the kick model neutron deficit approaches the experimental values if heuristic mode structures are included in the analyzes to account for lower frequency modes.

There are some additional adjustable parameters of the kick model we varied to confirm the results such as the implementation of the kicks over the drift EP orbits and the AE amplitudes. The results are pretty much insensitive to the choice of the kicks on EP orbits whereas the amplitudes of AEs in DIIID plasma are already at the upper limit of the expected $\delta B/B$ values measured throughout DIIID discharges with similar Alfvénic activity.

Finally we would like to illustrate the point we made in section 2.1 that realistic calculations of neutron rate are consistent with the used approximation of the neutron rate in CGM where the neutron flux is proportional to the product of thermal ion and beam ion densities. We take the DIIID analyzed cases shown in figure 4(*a*) as computed by the kick model. The model is already integrated in TRANSP and can be utilized here. We show in figure 8 how TRANSP computed neutron deficit with accurate neutron fluxes compares with the

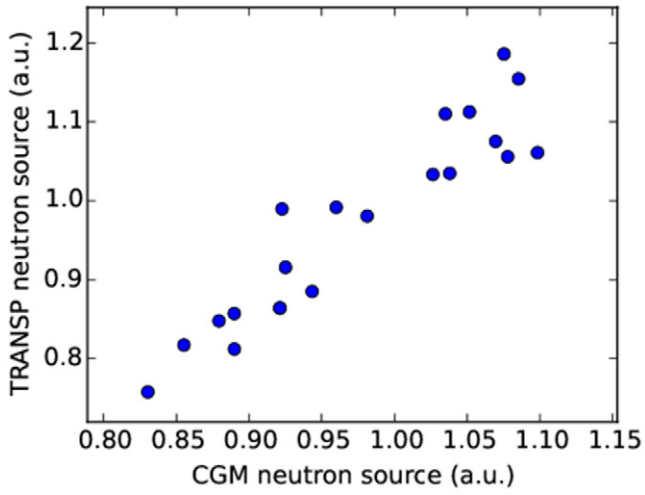

Figure 8. The proportionality of the neutron source used in TRANSP and its approximation used in CGM. Both values for each analyzed point of Alfvénic activity in DIIID plasma show in figure 4(*a*).

CGM approximation when the neutron flux is computed as a product of thermal ion and beam ion densities times the normalization constant. One can see that for all analyzed cases with and without (classical predictions in figure 4(*a*) denoted as Measured/TRANSP) Alfvénic activity the proportionality is clearly recovered. This means that CGM model does not introduce any unexpected modification of the neutron deficit and is properly used for its validation. There are some scattering of the points which we attribute to the statistical noise.

6. Summary

We presented and applied the perturbative and non-perturbative critical gradient models to DIII-D and NSTX plasmas for validations. The models agree to each other and seem to capture the level of neutron flux deficits in the presence of the Alfvénic modes. The perturbative CGM model predicts the neutron deficit in NSTX shot #141711 within the measurements error bars as compared with TRANSP modeling. However CGM neutron flux deficit in DIII-D shot #153072 differs from the measured deficit within a factor of two. This prediction follows from both perturbative and non-perturbative CGMs. The same level of discrepancy is observed for kick model computed deficit for DIII-D shot when only the Alfvénic modes are included. We point out at the potential improvement of the model by bringing in the eigenmodes with the Alfvén-acoustic polarization [37] which we did not find with the ideal MHD code NOVA.

The fundamental assumption of CGM is that the background plasma damping is not changed by the modes and thus weakly depends on the AE instability dynamics. It seems to be consistent with recent DIII-D observations. Even though CGM may not resolve all the details of fast ion distribution it has the same conclusion that the measured EP profiles on DIII-D are almost independent on the injection geometry. The large number of modes required for CGM implies the large number of overlapped resonances. This regime corresponds to near threshold excitation of AE instabilities when the collisional scattering frequency is much larger than the net growth rate [38]. It is hard to compare the conditions when the CGM is expected to work explicitly across the toroidal devices in general due to experimental uncertainties in the number of instabilities and in their internal amplitudes.

Nevertheless the level of agreement we observed is important as it points at the direction of a future research for the reduced model of the Alfvénic transport of fast ions. It justifies the development of more complete but still reduced 2D quasi-linear theory. The need to develop 2D QL model is listed as one of the most important problem for the near future EP physics research [3].

Acknowledgments

This material is based upon work supported by the U.S. Department of Energy, Office of Science, Office of Fusion Energy Sciences, using the DIII-D National Fusion Facility, a DOE Office of Science user facility. This work supported in part by DoE contracts No. DE-AC02-09CH11466, SC-G903402, DE-FC02-04ER54698. DIII-D data shown in this paper can be obtained in digital format by following the links at https://fusion.gat.com/global/D3D_DMP.

References

[1] Heidbrink W.W., Van Zeeland M.A., Austin M.E., Bass E.M., Ghantous K., Gorelenkov N.N., Grierson B.A., Spong D.A. and Tobias B.J. 2013 *Nucl. Fusion* **53** 093006
[2] Breizman B.N. and Sharapov S.E. 2011 *Plasma Phys. Control. Fusion* **53** 054001
[3] Gorelenkov N.N., Pinches S.D. and Toi K. 2014 *Nucl. Fusion* **54** 125001
[4] Aymar R. 2000 *Plasma Phys. Control. Fusion.* **42** B385
[5] Fasoli A. *et al* 2007 Progress in the ITER Physics Basis chapter 5: physics of energetic ions *Nucl. Fusion* **47** S264
[6] Ghantous K., Gorelenkov N.N., Berk H.L., Heidbrink W.W. and Van Zeeland M.A. 2012 *Phys. Plasmas* **19** 092511
[7] Berk H.L., Breizman B.N., Fitzpatrick J., Pekker M.S., Wong H.V. and Wong K.L. 1996 *Phys. Plasmas* **3** 1827
[8] Konies A. *et al* 2012 *Proc. 24th Int. Conf. on Fusion Energy (San Diego, 2012)* IAEA-CN-197/ITR/P1-34 www-naweb.iaea.org/napc/physics/FEC/FEC2012/index.htm
[9] Sharapov S.E. *et al* ITPA EP TG and JET-EFDA Contributors 2013 *Nucl. Fusion* **53** 104022
[10] Goldston R.J., McCune D.C., Towner H.H., Davis S.L., Hawryluk R.J. and Schmidt G.L. 1981 *J. Comput. Phys.* **43** 61
[11] Podestá M., Gorelenkova M.V. and White R.B. 2014 *Plasma Phys. Control. Fusion* **56** 055003
[12] Gorelenkov N.N., Berk H.L. and Budny R.V. 2005 *Nucl. Fusion* **45** 226
[13] Berk H.L. and Breizman B.N. 1994 *Advances in Plasma Physics: Thomas H. Stix Symposium* (*AIP Conf. Proc.* vol 314) ed N. J. Fisch (New York: AIP) p 140
[14] Berk H.L., Breizman B.N. and Pekker M.S. 1996 *Phys. Rev. Lett.* **76** 1256
[15] Cheng C.Z., Gorelenkov N.N. and Hsu C.T. 1995 *Nucl. Fusion* **35** 1639
[16] Cheng C.Z. and Gorelenkov N.N. 2004 *Phys. Plasmas* **11** 4784

[17] Mikkelsen D.R. 1989 *Nucl. Fusion* **29** 1113
[18] Fredrickson E.D. *et al* 2013 *Nucl. Fusion* **53** 013006
[19] White R.B., Gorelenkov N.N., Heidbrink W.W. and Van Zeeland M.A. 2010 *Plasma Phys. Control. Fusion* **53** 045012
[20] Gorelenkov N.N., Cheng C.Z. and Fu G.Y. 1999 *Phys. Plasmas* **6** 2802
[21] Berk H.L., Borba D.N., Breizman B.N., Pinches S.D. and Sharapov S.E. 2001 *Phys. Rev. Lett.* **87** 185002
[22] Borba D. *et al* and JET-EFDA Contributors 2010 *Proc. 23rd Int. Conf. on Fusion Energy (Daejeon, 2010)* (Vienna: IAEA) CD-ROM file IAEA-CN-180/THW/P7-08 www-naweb.iaea.org/napc/physics/FEC/FEC2010/index.htm
[23] Gorelenkov N.N. 2011 *11th IAEA Technical Committee Meeting Energetic Particles in Magnetic Confinement Systems (Austin, USA 7–10 September 2011)* http://w3fusion.ph.utexas.edu/ifs/iaeaep/
[24] Fu G.Y. and Cheng C.Z. 1992 *Phys. Fluids* B **4** 3722
[25] Breizman B.N. and Sharapov S.E. 1995 *Plasma Phys. Control. Fusion* **37** 1057
[26] Wang Z., Lin Z., Holod I., Heidbrink W.W., Tobias B., Van Zeeland M.A. and Austin M.E. 2013 *Phys. Rev. Lett.* **111** 145003
[27] Connor J.W., Hastie R.J. and Taylor J.B. 1979 *Proc. R. Soc.* A **365** 1
[28] White R.B. and Chance M.S. 1984 *Phys. Fluids* **27** 2455
[29] Pankin A. *et al* 2004 *Comput. Phys. Commun.* **159** 157
[30] Podestá M., Gorelenkova M.V., Darrow D.S., Fredrickson E.D., Gerhardt S.P. and White R.B. 2015 *Nucl. Fusion* **55** 053018
[31] Podestá M. *et al* 2012 *Nucl. Fusion* **52** 094001
[32] Menard J.E. *et al* 2006 *Phys. Rev. Lett.* **97** 095002
[33] Kramer G.J. *et al* 2006 *Phys. Plasmas* **13** 056104
[34] Cheng C.Z. 1992 *Phys. Rep.* **211** 1
[35] Heidbrink W.W. *et al* 2014 *Plasma Phys. Control. Fusion* **56** 095030
[36] Lao L.L., John H.S., Stambaugh R.D., Kellman A.G. and Pfeiffer W. 1985 *Nucl. Fusion* **25** 1611
[37] Gorelenkov N. N., Van Zeeland M.A., Berk H.L., Crocker N.A., Darrow D., Fredrickson E., Fu G.-Y., Heidbrink W.W., Menard J. and Nazikian R. 2009 *Phys. Plasmas* **16** 056107
[38] Berk H.L., Breizman B.N. and Pekker M.S. 1997 *Plasma Phys. Rep.* **23** 778